Elsevier Editorial System(tm) for Colloids and Surfaces B: Biointerfaces

Manuscript Draft

Manuscript Number: COLSUB-D-16-02344R1

Title: Nucleotide-directed syntheses of gold nanohybrid systems with structure-dependent optical features: Selective fluorescence sensing of Fe3+ ions

Article Type: Full Length Article

Keywords: adenosine monophosphate; gold nanoclusters; gold nanoparticles; fluorescence quenching; iron ion; biosensor

Corresponding Author: Dr. Imre Dekany, DSc.

Corresponding Author's Institution: University of Szeged

First Author: Ditta Ungor

Order of Authors: Ditta Ungor; Edit Csapó, PhD; Barbara Kismárton; Ádám Juhász; Imre Dekany, DSc.

Manuscript Region of Origin: HUNGARY

Abstract: This study demonstrates a one-step synthesis for the preparation of both adenosine monophosphate (AMP)-stabilized colloidal gold nanoparticles (AMP-Au NPs) and fluorescent gold nanoclusters (AMP-Au NCs). The dominant role of AMP:$AuCl_4^-$ molar ratios in the formation of diverse nanosized Au products was proved. The size, the structure and the unique structure-dependent optical properties of the NPs and NCs were determined based on the results of numerous spectroscopic (UV-visible, fluorescence, infrared, x-ray photoelectron), high resolution electron microscopy (HRTEM) and dynamic light scattering (DLS) techniques. Stabile AMP-Au NPs with diameter of ca. 11 nm and ultra-small AMP-Au NCs having blue fluorescence (λ_{em} = 480 nm) were identified. In addition, the AMP-Au NCs have been utilized to develop a selective sensor for the detection of Fe3+ ions in aqueous medium based on fluorescence quenching. Several essential metal ions and anions have been tested but our results clearly supported that dominant quenching was observed only for Fe3+ ions. Based on the determined limit of detection (LOD = 2.0 μM) our system is capable of detecting Fe3+ ions in drinking water. The Stern-Volmer constants (K_{SV}) and various thermodynamic parameters (ΔG, ΔH°, ΔS°, ΔCp) of the quenching process have also been determined by the Stern-Volmer fitting of the fluorescence data in order to better understand the quenching mechanism.

Response to Reviewers: Response to each point of the comments of the Editor and Reviewers

We are very grateful to the Editor and Reviewers for their efforts to improve our manuscript. Below, we give our point-by-point responses to the points raised by the Editor and the Reviewers, and also the changes made in the manuscript.

In response to the comments of the Editor.

Comment
1. “Please read the paper carefully for English language style, grammar and spelling, and make appropriate corrections and changes.”
The manuscript has been completely rewritten. Corrections are marked in red and only the significant grammar and spelling changes were listed below.

Comment
2. “Please provide a BRIEF caption for the graphical abstract”.
Minimal corrections were made in graphical abstract and a legend is also given.

Comment
3. “Please provide error bars (with definition eg SD, n=?) on figures where numerical data are shown. This information should be included in the figure captions. For figures where error bars are already shown the bars should be explained in the figure captions.
In the case of Fig. 5, 6, 7 and Table 1 the appropriate error bars were presented in the Figures and in the Figure captions as well.

Comment
4. Please include a list of changes in the manuscript and a response to each point raised by the reviewers AND THE EDITOR when you submit the revised manuscript. The list must indicate your changes by page and line number in the revised manuscript. These changes should be shown in colour in the manuscript. THESE ARE ABSOLUTE REQUIREMENTS FOR RE-CONSIDERATION OF YOUR PAPER.
The changes are indicated in red. The list of changes in the manuscript and a response to each point raised by the Reviewers and the Editor are enclosed.

The authors are grateful for the valuable remarks of the Reviewer #1.
Comment
1. “the text should be checked by the native English language speaker”
The manuscript has been completely rewritten. Corrections are marked in red and only the significant grammar and spelling changes were listed below.

Comment
2. “p.4 red wine colour of the samples (p.4) suggests the formation of nanorods. Did authors try to determine the shape of nanoparticles, and how it can influence nanohybrid formation?”
Red wine colour of the samples indicates the formation of colloidal gold nanoparticles. The shape, the size and the size distribution of the particles have been determined by HRTEM and DLS techniques as presented in Fig. 1. These results confirmed the formation of spherical particles with the average size of ca. 11 nm. Moreover, the characteristic plasmon band (Fig. 1.a) of the synthesized gold nanoparticles also indicates the presence of spherical particles. The gold nanorods have two characteristic plasmon bands in the UV-Vis spectra, where the second peak depends on the aspect ratio of the rod.

Comment
3. “having DLS, why size distribution of NP's is not shown?”
The shape, the size and the size distribution of the particles have been determined by HRTEM and DLS techniques. Fig 1. represents a HRTEM image of the AMP-stabilized gold nanoparticles, the representative size

distribution of these particles was presented in the Graphical abstract. Because of the limited number of figures only the hydrodynamic data with the corresponding standard deviations as well as the Zeta-potential value were summarized in page 8. The size distribution of the gold nanoparticles determined by DLS is presented here.

Comment

4. "I do not understand why quenching constant is treated as equilibrium constant? They cannot be the same. Gibbs free energy change DG0 is calculated for standard state. What is the standard state for Fe+3 ions and Au NP's? What is the reaction, for which authors want to derive equilibrium constant? This does not make sense to me. Of course, one can obtain any desired constant from the experiment, but why to call it equilibrium constant? Relation DG0 = -RT ln K makes sense only for reaction, in which components have specified standard state. p.8 spontaneous reaction can be also endothermic, be careful with generalization."

First, we accept the comment of Reviewer#1, unfortunately the ΔG was presented as standard value; the correct notation is ΔG instead of ΔG°. The ΔH° and ΔS° are standard data.

Secondly, in case of static quenching the Stern-Volmer quenching constant is known as binding or association constant (Lakowicz, J. R.: Principles of Fluorescence Spectroscopy, 3rd ed. Springer Science, New York, 2006, Zheng C. et al. Study on the interaction between histidine-capped Au nanoclusters and bovine serum albumin with spectroscopic techniques, Spectro Chim Act A, 2014, 118:897-902). In our manuscript the modified Stern-Volmer-based evaluation process was also inserted into the text. In view of the KSV the appropriate Ka values were also calculated and using the van't Hoff equation the thermodynamic parameters were refined (page 8-9). Moreover, the interpretation of the thermodynamic parameters which refers to the problematic sentence (data relating to the spontaneous reaction) were discussed more on the page 9 line 1-11.

"The determined thermodynamic data are summarized in Table 1 based on the integrated van't Hoff analysis (Eq. 3). Fig.7a. shows that linear (grey dashed line) and nonlinear (black dashed line) regression methods were also used to fit the experimental data [Adam cikk]. It was found that instead of the widely applied linear regression, in our case the nonlinear regression method provides the best correlation of the experimental data. Namely, in the case of the linear regression the calculated coefficient is 0.9022 while for nonlinear regression the coefficient is 0.9823. The negative values of ΔG (ca. -29 kJ mol-1 depending on the temperature) indicate that the reactions between the AMP-Au NCs and Fe3+ ions are thermodynamically favorable. The negative ΔH° (-84.57±8.46 kJ mol-1) suggests the fact that the binding reaction is exothermic. Since, it was established that the $\Delta H^\circ < 0$ and $\Delta S^\circ < 0$ and also the $|\Delta H^\circ| > |T\Delta S^\circ|$ most probably the reaction is spontaneous and is enthalpy-driven [35]. The detemined ΔCp is -4.86±1.17 kJ mol-1K-1."

The authors thank for Reviewer #2 the valuable remarks.

Comment

1." However, the paper is not particularly well written and English should be improved. There are several misprints and grammatical errors and the whole manuscript should be checked carefully."

The manuscript has been completely rewritten. Corrections are marked in red and only the significant grammar and spelling changes were listed below.

Comment

2. “Generally my main concern is the interpretation of the kinetic results obtained on the basis of the Stern-Volmer model. This is very important point and the corresponding paragraph in the text and the Table 1 are not clearly written. Here are some remarks: From Table 1 I understand that the obtained thermodynamic constant are not standard values, while in the text (p. 8, eq. 2) they are presented as standard quantities. Moreover, these results are in the text interpreted only qualitatively (the thermodynamic parameters are negative) and not qualitatively. The obtained enthalpy and entropy values are correct if they are constant in the examined temperature region. Is that fulfilled? All these comments should be clarified and the corresponding paragraph in the text should be modified accordingly.
.”
We accept the comment of Reviewer#2, unfortunately the ΔG was presented as standard value; the correct notation is ΔG instead of ΔG°. The ΔH° and ΔS° are standard data because they were measured at various temperatures. Moreover, the interpretation of the thermodynamic parameters were discussed more on the page 9 line 1-11.
“The determined thermodynamic data are summarized in Table 1 based on the integrated van’t Hoff analysis (Eq. 3). Fig.7a. shows that linear (grey dashed line) and nonlinear (black dashed line) regression methods were also used to fit the experimental data [Adam cikk]. It was found that instead of the widely applied linear regression, in our case the nonlinear regression method provides the best correlation of the experimental data. Namely, in the case of the linear regression the calculated coefficient is 0.9022 while for nonlinear regression the coefficient is 0.9823. The negative values of ΔG (ca. -29 kJ mol-1 depending on the temperature) indicate that the reactions between the AMP-Au NCs and Fe3+ ions are thermodynamically favorable. The negative ΔH° (-84.57±8.46 kJ mol-1) suggests the fact that the binding reaction is exothermic. Since, it was established that the ΔH° < 0 and ΔS° < 0 and also the |ΔH°| > |TΔS°| most probably the reaction is spontaneous and is enthalpy-driven [35]. The detemined ΔCp is -4.86±1.17 kJ mol-1K-1.”
The Stern-Volmer-based evaluation process was also completed (page 8, line 8-18)
The authors thank for Reviewer #3 the valuable remarks.
Comment
1.”However, I'd suggest that the authors should concentrate mostly on the Au clusters, which are significantly more interesting given their further analytical applications. Accordingly, Figure 1 should be moved to the Supporting Info section or dropped, whereas Figure S4 should be moved to the main text. It should be interesting to explicitly write what is the hydrodynamic radius of the clusters under various pHs and ionic strengths. Also, information about the electrophoretic mobility (zeta potential) and the stability of the clusters in solutions containing various cations, especially Fe3+ as a function of the temperature should be provided. “
We accept the comment of Reviewer#3, the manuscript was completed with some important data relating to the electrophoretic mobility (zeta potential), the size and the stability of the clusters in solutions. (page 7, line 11-25)
The following data were inserted into the text: “Besides the structural characterization the pH-stability of the AMP-Au NCs has also been investigated in a wide pH range (pH 1-12). As it can be seen in Fig. S3a, below pH 6.0 and above pH 9.0 the fluorescence intensity of the AMP-Au NCs continually decreases. This observation is in good agreement with the change of the size and the Zeta-potential values of the nanoclusters determined by DLS. The hydrodynamic diameter of the AMP-Au NCs is 0.71 ±

0.1 nm (PDI = 0.181) at pH 6.0. Fig. S3b clearly represents that in the pH range of 6.0-9.0 the size does not change measurable and the Zeta potential values are in the range of -35 –(-25) mV indicating the presence of stabile system. Below pH 6 the size of these clusters starts to increase and the absolute value of Zeta-potentials also decreases to 5-10 mV which confirm the formation of aggregated particles at acidic conditions. At strong acidic media (pH 1-2) fast aggregation was also observed, which is followed by DLS studies. The measured hydrodynamic diameter gradually increases in time (Fig. S4). In conclusion we established that synthesized blue-emitting AMP-Au NCs show high kinetic stability in the pH range of 6.0-9.0, where the PL intensity, the size and the Zeta-potential values are nearly constant."
Our opinion is that the one-step preparation route of AMP-stabilized gold nanoparticles is also important, so the Figure 1 does not move to Supplementary file. Because of the limited number of Figures the hydrodynamic data with the corresponding standard deviations as well as the Zeta-potential values of the clusters as a function of pH were presented in Fig. S3b.

Comment
2." Although it is maintained that the detection limit is 2 micromoles, Fig. 6 suggests that a reasonable accuracy of measurements is only attained for Fe3+ concentration about 10 µM where ordinary analytical methods work well. Therefore, the advantage of the proposed fluorescence method should be better explained."
Fig. 6.b presents only the dynamic range of the studied systems. In case of the determination of LOD value wider concentration range (100 nM – 1 mM) was examined and measurable fluorescence quenching was obtained for cFe3+ = 2.0 µM. This missing experimental information was presented on page 5, line 8-9.
However, the generally used analytical methods have better LOD value but our methods is suitable for rapid feedback on the iron content of the tested aqueous samples. This method requires a few amount of fluorescent sample and does not contain any toxic reagents. Moreover, the AMP-Au NCs have excellent selectivity for Fe3+. These properties give a great opportunity to develop a cost-effective, rapid and high selectivity iron-chemosensors for the detection the iron content in water and in biological samples.

Comment
3."The physics behind the calculations of the quenching constant and (Eq.(1)) should be discussed in more detail. What was the influence of the temperature and corresponding viscosity changes on the fluorescence spectra of clusters and the Io value? Also the mechanism of the specific activity of the Fe3+ ions should be discussed."
Firstly, the temperature has no dominant effect on the I0 value of the AMP-Au NCs (only 10-12 % differences were obtained in the range of 298-323 K). Furthermore, the corresponding I0 values were registered in all cases (at 298, 303, 310 and 323 K). Secondly, the viscosity of the samples did not change measurable; quite similar values were determined as for pure water.
Most probably, the Fe3+ ions are bonded onto the surface of nanoclusters via the AMP molecules. Although, the N7 position of the AMP is probably occupied by the gold atom, but it has additional coordination sites, which can bind the Fe3+ ions. The Zeta-potential values of the clusters before (ca. -35 mV) and after (ca. + 30 mV) addition of Fe3+ ions also confirm the strong binding of metal ions onto the cluster surface.

The list of changes in the manuscript:
In the text
page 1, Abstract: Several sentences were corrected. (line 12, 15-18)
page 2, Introduction: line 5, 6, 7, 9, 12-14, 18, 22-24, 25-30
page 3, Introduction: line 3-5, 11, 13-16
page 3, Materials: line 23-24.
page 4, Preparation of AMP-Au NCs and AMP-Au NPs: line 2,3, 5-7,
page 5, Fluorescence sensing of Fe3+by using AMP-Au NCs: line 5, 8, 11.
page 5, Results and discussion: line 16-18,
page 7, Results and discussion: line 12-21, 24, 25, 27.
page 8, Results and discussion: line 14-25.
page 9, Results and discussion: line 1-11, 17-22.
page 9, Conclusions: line 28, 30, 33-35
page 10, Conclusions: line 1-4.
page 10, Acknowledgement: line 7-10.
Tables: Ka values were inserted into the Table 1, and the thermodynamic parameters were refined.
Tables and Figures captions
Figure 5 and Figure 7 were slightly modified.
Figures
Figure 5 and Figure 7 were slightly modified.
Graphical abstract
Minimal corrections were made in graphical abstract and a legend is also given.
4 new references were also cited.

Once again, we are grateful to the Editor and the Reviewers for their efforts to improve our manuscript.
Yours sincerely,
Edit Csapó and Imre Dékány
corresponding authors

MAGYAR TUDOMÁNYOS AKADÉMIA
Szupramolekuláris és Nanoszerkezetű Anyagok Kutatócsoport
SZEGEDI TUDOMÁNYEGYETEM
6720 Szeged, Dóm tér 8.
Tel.: +62 545 136 Fax: +62 545 971

HUNGARIAN ACADEMY OF SCIENCES
Supramolecular and Nanostructured Materials Research Group
UNIVERSITY OF SZEGED
Dóm tér 8., Szeged, H-6720, Hungary
Phone: +62 545 136 Fax: +62 545 971

Prof. John L. Brash

Editor of Colloids and Surfaces B

McMaster University, Hamilton, Ontario, Canada

17 March, 2017.

Dear Prof. Brash!

According to some comments received from Editor and Reviewers we have revised our manuscript (**COLSUB-D-16-02344**, *Nucleotide-directed syntheses of gold nanohybrid systems with structure-dependent optical features: Selective fluorescence sensing of Fe3+ ions*
Authors: Ditta Ungor, Edit Csapó*, Barbara Kismárton, Ádám Juhász, Imre Dékány*
Attached please find the responses to Editor and Reviewers suggestions and questions.

In the name of all co-authors I would like to thank you for the time and efforts while treating our submission.

Yours sincerely,

Edit Csapó and Imre Dékány

corresponding authors

Response to each point of the comments of the Editor and Reviewers

We are very grateful to the Editor and Reviewers for their efforts to improve our manuscript. Below, we give our point-by-point responses to the points raised by the Editor and the Reviewers, and also the changes made in the manuscript.

In response to the comments of the **Editor**.

Comment

1. "Please read the paper carefully for English language style, grammar and spelling, and make appropriate corrections and changes."

The manuscript has been completely rewritten. Corrections are marked in red and only the significant grammar and spelling changes were listed below.

Comment

2. "Please provide a BRIEF caption for the graphical abstract".

Minimal corrections were made in graphical abstract and a legend is also given.

Comment

3. "Please provide error bars (with definition eg SD, n=?) on figures where numerical data are shown. This information should be included in the figure captions. For figures where error bars are already shown the bars should be explained in the figure captions.

In the case of Fig. 5, 6, 7 and Table 1 the appropriate error bars were presented in the Figures and in the Figure captions as well.

Comment

4. Please include a list of changes in the manuscript and a response to each point raised by the reviewers AND THE EDITOR when you submit the revised manuscript. The list must indicate your changes by page and line number in the revised manuscript. These changes should be shown in colour in the manuscript. THESE ARE ABSOLUTE REQUIREMENTS FOR RE-CONSIDERATION OF YOUR PAPER.

The changes are indicated in red. The list of changes in the manuscript and a response to each point raised by the Reviewers and the Editor are enclosed.

The authors are grateful for the valuable remarks of the **Reviewer #1**.

Comment

1. "the text should be checked by the native English language speaker"

The manuscript has been completely rewritten. Corrections are marked in red and only the significant grammar and spelling changes were listed below.

Comment

2. "p.4 red wine colour of the samples (p.4) suggests the formation of nanorods. Did authors try to determine the shape of nanoparticles, and how it can influence nanohybrid formation?"

Red wine colour of the samples indicates the formation of colloidal gold nanoparticles. The shape, the size and the size distribution of the particles have been determined by HRTEM and DLS techniques as presented in Fig. 1. These results confirmed the formation of spherical particles with the average size of *ca*. 11 nm. Moreover, the characteristic plasmon band (Fig. 1.a) of the synthesized gold nanoparticles also indicates the presence of spherical particles. The gold nanorods have two characteristic plasmon bands in the UV-Vis spectra, where the second peak depends on the aspect ratio of the rod.

Comment

3. "having DLS, why size distribution of NP's is not shown?"

The shape, the size and the size distribution of the particles have been determined by HRTEM and DLS techniques. Fig 1. represents a HRTEM image of the AMP-stabilized gold nanoparticles, the representative size distribution of these particles was presented in the Graphical abstract. Because of the limited number of figures only the hydrodynamic data with the corresponding standard deviations as well as the Zeta-potential value were summarized in page 8. The size distribution of the gold nanoparticles determined by DLS is presented here.

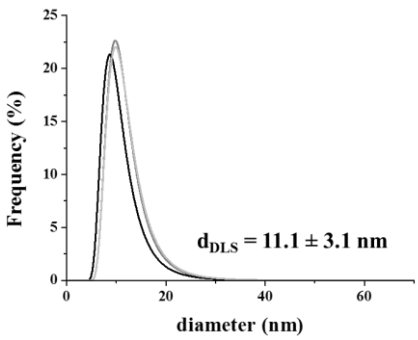

Fig. R1. Size distribution of the AMP-stabilized gold nanoparticles determined by DLS

Comment

4. "I do not understand why quenching constant is treated as equilibrium constant? They cannot be the same. Gibbs free energy change DG0 is calculated for standard state. What is the standard state for Fe+3 ions and Au NP's? What is the reaction, for which authors want to derive equilibrium constant? This does not make sense to me. Of course, one can obtain any desired constant from the experiment, but why to call it equilibrium constant? Relation DG0 = -RT ln K makes sense only for reaction, in which components have specified standard state. p.8 spontaneous reaction can be also endothermic, be careful with generalization."

First, we accept the comment of Reviewer#1, unfortunately the ΔG was presented as standard value; the correct notation is ΔG instead of ΔG°. The ΔH° and ΔS° are standard data.

Secondly, in case of static quenching the Stern-Volmer quenching constant is known as binding or association constant (*Lakowicz, J. R.: Principles of Fluorescence Spectroscopy, 3rd ed. Springer Science, New York, 2006, Zheng C. et al. Study on the interaction between histidine-capped Au nanoclusters and bovine serum albumin with spectroscopic techniques, Spectro Chim Act A, 2014, 118:897-902*). In our manuscript the modified Stern-Volmer-based evaluation process was also inserted into the text. In view of the K_{SV} the appropriate K_a values were also calculated and using the van't Hoff equation the thermodynamic parameters were refined (page 8-9). Moreover, the interpretation of the thermodynamic parameters which refers to the problematic sentence (data relating to the spontaneous reaction) were discussed more on the page 9 line 1-11.

"The determined thermodynamic data are summarized in ***Table 1*** *based on the integrated van't Hoff analysis (****Eq. 3****).* ***Fig.7a****. shows that linear (grey dashed line) and nonlinear (black dashed line) regression methods were also used to fit the experimental data [Adam cikk]. It was found that instead of the widely applied linear regression, in our case the nonlinear regression method provides the best correlation of the experimental data. Namely, in the case of the linear regression the calculated coefficient is 0.9022 while for nonlinear regression the coefficient is 0.9823. The negative values of* ΔG *(ca. -29 kJ* mol^{-1} *depending on the temperature) indicate that the reactions between the AMP-Au NCs and* Fe^{3+} *ions are thermodynamically favorable. The negative* $\Delta H°$ *(-84.57±8.46 kJ* mol^{-1}*) suggests the fact that the binding reaction is exothermic. Since, it was established that the* $\Delta H° < 0$ *and* $\Delta S° < 0$

and also the $|\Delta H°| > |T\Delta S°|$ most probably the reaction is spontaneous and is enthalpy-driven [35]. The detemined ΔC_p is -4.86±1.17 kJ mol^{-1}K^{-1}."

The authors thank for **Reviewer #2** the valuable remarks.

Comment

1." However, the paper is not particularly well written and English should be improved. There are several misprints and grammatical errors and the whole manuscript should be checked carefully."

The manuscript has been completely rewritten. Corrections are marked in red and only the significant grammar and spelling changes were listed below.

Comment

2. "Generally my main concern is the interpretation of the kinetic results obtained on the basis of the Stern-Volmer model. This is very important point and the corresponding paragraph in the text and the Table 1 are not clearly written. Here are some remarks: From Table 1 I understand that the obtained thermodynamic constant are not standard values, while in the text (p. 8, eq. 2) they are presented as standard quantities. Moreover, these results are in the text interpreted only qualitatively (the thermodynamic parameters are negative) and not qualitatively. The obtained enthalpy and entropy values are correct if they are constant in the examined temperature region. Is that fulfilled? All these comments should be clarified and the corresponding paragraph in the text should be modified accordingly.

."

We accept the comment of Reviewer#2, unfortunately the ΔG was presented as standard value; the correct notation is ΔG instead of ΔG°. The ΔH° and ΔS° are standard data because they were measured at various temperatures. Moreover, the interpretation of the thermodynamic parameters were discussed more on the page 9 line 1-11.

*"The determined thermodynamic data are summarized in **Table 1** based on the integrated van't Hoff analysis (**Eq. 3**). **Fig.7a**. shows that linear (grey dashed line) and nonlinear (black dashed line) regression methods were also used to fit the experimental data [Adam cikk]. It was found that instead of the widely applied linear regression, in our case the nonlinear regression method provides the best correlation of the experimental data. Namely, in the case of the linear regression the calculated coefficient is 0.9022 while for nonlinear*

regression the coefficient is 0.9823. The negative values of ΔG *(ca. -29 kJ mol*$^{-1}$ *depending on the temperature) indicate that the reactions between the AMP-Au NCs and* Fe^{3+} *ions are thermodynamically favorable. The negative* $\Delta H°$ *(-84.57±8.46 kJ mol*$^{-1}$*) suggests the fact that the binding reaction is exothermic. Since, it was established that the* $\Delta H° < 0$ *and* $\Delta S° < 0$ *and also the* $|\Delta H°| > |T\Delta S°|$ *most probably the reaction is spontaneous and is enthalpy-driven [35]. The detemined* ΔC_p *is -4.86±1.17 kJ mol*$^{-1}$*K*$^{-1}$*."*

The Stern-Volmer-based evaluation process was also completed (page 8, line 8-18)

"Based on the Stern-Volmer fitting [39] of the fluorescence data the quenching constant (K_{SV}*) can be determined according to the* ***Eq. 1****, where* $\boldsymbol{I_0}$ *and* ***I*** *is the maximum of the fluorescence intensity before and after the addition of* Fe^{3+} *and [Q] is the equilibrium concentration of* Fe^{3+}*.*[1]

$$I_0/I = 1 + K_{SV}[Q] \qquad (1)$$

If we plotted the I_0/I *as a function of* c_{Fe3+} ***(Fig. 6b)*** *the slope of the curve gives the corresponding* K_{SV}*. Using the modified Stern-Volmer equation (****Eq. 2****) [HSA CdTe] the* K_a *binding constants were also calculated (*$I_0/(I_0-I)$ *vs.* $[Q]^{-1}$*) and the values were summarized in* ***Table 1****.*

$$I_0/\Delta I = 1/f_a + 1/f_a K_a [Q]^{-1} \qquad (2)$$

where the $\boldsymbol{\Delta I = I_0 - I}$*,* $\boldsymbol{f_a}$ *is the mole fraction of solvent accessible AMP-Au NCs,* $\boldsymbol{K_a}$ *is analogous to the associative binding constant."*

The authors thank for **Reviewer #3** the valuable remarks.

Comment

1."However, I'd suggest that the authors should concentrate mostly on the Au clusters, which are significantly more interesting given their further analytical applications. Accordingly, Figure 1 should be moved to the Supporting Info section or dropped, whereas Figure S4 should be moved to the main text. It should be interesting to explicitly write what is the hydrodynamic radius of the clusters under various pHs and ionic strengths. Also, information about the electrophoretic mobility (zeta potential) and the stability of the clusters in solutions containing various cations, especially Fe3+ as a function of the temperature should be provided. "

[1] If the value of K_{SV} is large enough and the Stern-Vollmer plot is linear instead of the equilibrium concentration of the quencher the analytical concentration is also useable.

We accept the comment of Reviewer#3, the manuscript was completed with some important data relating to the electrophoretic mobility (zeta potential), the size and the stability of the clusters in solutions. (page 7, line 11-25)

The following data were inserted into the text: *"Besides the structural characterization the pH-stability of the AMP-Au NCs has also been investigated in a wide pH range (pH 1-12). As it can be seen in* ***Fig. S3a****, below pH 6.0 and above pH 9.0 the fluorescence intensity of the AMP-Au NCs continually decreases. This observation is in good agreement with the change of the size and the Zeta-potential values of the nanoclusters determined by DLS. The hydrodynamic diameter of the AMP-Au NCs is 0.71 ± 0.1 nm (PDI = 0.181) at pH 6.0. Fig. S3b clearly represents that in the pH range of 6.0-9.0 the size does not change measurable and the Zeta potential values are in the range of -35 –(-25) mV indicating the presence of stabile system. Below pH 6 the size of these clusters starts to increase and the absolute value of Zeta-potentials also decreases to 5-10 mV which confirm the formation of aggregated particles at acidic conditions. At strong acidic media (pH 1-2) fast aggregation was also observed, which is followed by DLS studies. The measured hydrodynamic diameter gradually increases in time (****Fig. S4****). In conclusion we established that synthesized blue-emitting AMP-Au NCs show high kinetic stability in the pH range of 6.0-9.0, where the PL intensity, the size and the Zeta-potential values are nearly constant."*

Our opinion is that the one-step preparation route of AMP-stabilized gold nanoparticles is also important, so the Figure 1 does not move to Supplementary file. Because of the limited number of Figures the hydrodynamic data with the corresponding standard deviations as well as the Zeta-potential values of the clusters as a function of pH were presented in Fig. S3b.

Comment

2." Although it is maintained that the detection limit is 2 micromoles, Fig. 6 suggests that a reasonable accuracy of measurements is only attained for Fe3+ concentration about 10 µM where ordinary analytical methods work well. Therefore, the advantage of the proposed fluorescence method should be better explained."

Fig. 6.b presents only the dynamic range of the studied systems. In case of the determination of LOD value wider concentration range (100 nM – 1 mM) was examined and measurable fluorescence quenching was obtained for c_{Fe3+} = 2.0 µM. This missing experimental information was presented on page 5, line 8-9.

However, the generally used analytical methods have better LOD value but our

methods is suitable for rapid feedback on the iron content of the tested aqueous samples. This method requires a few amount of fluorescent sample and does not contain any toxic reagents. Moreover, the AMP-Au NCs have excellent selectivity for Fe^{3+}. These properties give a great opportunity to develop a cost-effective, rapid and high selectivity iron-chemosensors for the detection the iron content in water and in biological samples.

Comment

3."The physics behind the calculations of the quenching constant and (Eq.(1)) should be discussed in more detail. What was the influence of the temperature and corresponding viscosity changes on the fluorescence spectra of clusters and the Io value? Also the mechanism of the specific activity of the Fe3+ ions should be discussed."

Firstly, the temperature has no dominant effect on the I_0 value of the AMP-Au NCs (only 10-12 % differences were obtained in the range of 298-323 K). Furthermore, the corresponding I_0 values were registered in all cases (at 298, 303, 310 and 323 K). Secondly, the viscosity of the samples did not change measurable; quite similar values were determined as for pure water.

Most probably, the Fe^{3+} ions are bonded onto the surface of nanoclusters via the AMP molecules. Although, the N7 position of the AMP is probably occupied by the gold atom, but it has additional coordination sites, which can bind the Fe^{3+} ions. The Zeta-potential values of the clusters before (ca. -35 mV) and after (ca. + 30 mV) addition of Fe^{3+} ions also confirm the strong binding of metal ions onto the cluster surface.

The list of changes in the manuscript:

In the text

page 1, Abstract: Several sentences were corrected. (line 12, 15-18)

page 2, Introduction: line 5, 6, 7, 9, 12-14, 18, 22-24, 25-30

page 3, Introduction: line 3-5, 11, 13-16

page 3, Materials: line 23-24.

page 4, Preparation of AMP-Au NCs and AMP-Au NPs: line 2,3, 5-7,

page 5, Fluorescence sensing of $Fe^{3+}$by using AMP-Au NCs: line 5, 8, 11.

page 5, Results and discussion: line 16-18,

page 7, Results and discussion: line 12-21, 24, 25, 27.

page 8, Results and discussion: line 14-25.

page 9, Results and discussion: line 1-11, 17-22.

page 9, Conclusions: line 28, 30, 33-35

page 10, Conclusions: line 1-4.

page 10, Acknowledgement: line 7-10.

Tables: K_a values were inserted into the Table 1, and the thermodynamic parameters were refined.

Tables and Figures captions

Figure 5 and Figure 7 were slightly modified.

Figures

Figure 5 and Figure 7 were slightly modified.

Graphical abstract

Minimal corrections were made in graphical abstract and a legend is also given.

4 new references were also cited.

Once again, we are grateful to the Editor and the Reviewers for their efforts to improve our manuscript.

Yours sincerely,

Edit Csapó and Imre Dékány

corresponding authors

Highlights

- Adenosine-monophosphate-directed synthesis of gold NPs was carried out at 37 °C.
- AMP-stabilized gold nanoclusters having blue fluorescence were fabricated at 37 °C.
- AMP-Au NPs and NCs possess high kinetic stability under physiological conditions.
- AMP-Au NCs detect the Fe^{3+} at 2 μM in aqueous medium via fluorescence quenching.
- Thermodynamic aspects of the static quenching process were characterized.

Nucleotide-directed syntheses of gold nanohybrid systems with structure-dependent optical features: Selective fluorescence sensing of Fe^{3+} ions

Ditta Ungor[a], Edit Csapó[a,b,*], Barbara Kismárton[a], Ádám Juhász[a,b], Imre Dékány[a,*]

[a] MTA-SZTE Supramolecular and Nanostructured Materials Research Group, Department of Medical Chemistry, Faculty of Medicine, University of Szeged, H-6720 Dóm square 8, Szeged, Hungary

[b] Department of Physical Chemistry and Materials Sciences, University of Szeged, H-6720, Aradi v.t.1, Szeged, Hungary

[*]Corresponding authors: Department of Medical Chemistry, Faculty of Medicine, University of Szeged, H-6720 Dóm square 8, Szeged, Hungary, Tel.: +36 62 544476
E-mail addresses: juhaszne.csapo.edit@med.u-szeged.hu (E. Csapó), i.dekany@chem.u-szeged.hu (I. Dékány)

Abstract

This study demonstrates a one-step synthesis for the preparation of both adenosine monophosphate (AMP)-stabilized colloidal gold nanoparticles (AMP-Au NPs) and fluorescent gold nanoclusters (AMP-Au NCs). The dominant role of AMP:$AuCl_4^-$ molar ratios in the formation of diverse nanosized Au products was proved. The size, the structure and the unique structure-dependent optical properties of the NPs and NCs were determined based on the results of numerous spectroscopic (UV-visible, fluorescence, infrared, x-ray photoelectron), high resolution electron microscopy (HRTEM) and dynamic light scattering (DLS) techniques. Stabile AMP-Au NPs with diameter of *ca*. 11 nm and ultra-small AMP-Au NCs having blue fluorescence (λ_{em} = 480 nm) were identified. In addition, the AMP-Au NCs have been utilized to develop a selective sensor for the detection of Fe^{3+} ions in aqueous medium based on fluorescence quenching. Several essential metal ions and anions have been tested but our results clearly supported that dominant quenching was observed only for Fe^{3+} ions. Based on the determined limit of detection (LOD = 2.0 µM) our system is capable of detecting Fe^{3+} ions in drinking water. The Stern-Volmer constants (K_{SV}) and various thermodynamic parameters (ΔG, $\Delta H°$, $\Delta S°$, ΔC_p) of the quenching process have also been determined by the Stern-Volmer fitting of the fluorescence data in order to better understand the quenching mechanism.

Keywords: adenosine monophosphate, gold nanoclusters, gold nanoparticles, fluorescence quenching, iron ion, biosensor

1. Introduction

Due to the unique shape-, size- and composition-dependent optical properties the noble metal nanostructures (mainly gold and silver) are widely used nanomaterials and they have been extensively investigated in different ways. The development of Au and silver (Ag) nanoparticles (NPs) - or nanoclusters (NCs) - based optical biosensors and bioimaging agents is a key area in the field of nanomedicine. [1–3]. In recent years, the biocompatible preparation routes of nanosized noble metal particles are in the focus of extensive research [4–7]. During this procedure only one biomolecule acts both as a reducing and a stabilizing agent [8,9] and different nanostructures (NPs or NCs) can be synthesized depending on the applied molar ratio of gold precursor ions (*e.g.* aurate) and the biomolecule [10,11]. Namely, the application of small biomolecule excess results in the formation of colloidal Au NPs (d > 2 nm) which possess characteristic size- and shape-dependent plasmon resonance band in the UV-Vis spectra. In contrast, for the utilization of high biomolecule excess subnanometer-sized Au NCs are formed (d < 2 nm) [12]. Besides the molar ratio of the reactants, the pH used in the synthesis also plays a determining role in the optical properties of the above mentioned nano-objects [13]. The ultra-small Au NCs show unique physical and chemical properties such as well-defined molecular structure, discrete electronic transitions and characteristic strong photoluminescence (PL) [14]. If the gold NCs consist of only a few-atoms (blue-emitting NCs) the appearance of the emission band mostly depends only on the number of metal atoms in the clusters [15,16]. Their PL lifetimes are usually on the order of nanoseconds although the surface ligands could have some influence on the fluorescence features. Furthermore, if the size of the NCs reaches the ~ 1.5-2.0 nm (red-emitting NCs) both the oxidation state of the surface metal atoms and the surface ligand effect influence the wavelength of the emission maximum. These NCs possess a characteristic PL in the orange/red (Vis) or in the near infrared (NIR) region and they have PL lifetime as well in the microsecond range [17,18]. Upon further increase in size, the few nanometer Au NPs (d > 2 nm) show plasmonic feature, because the collective oscillation of the free electron occurs. However, the smaller (d < 20-30 nm) plasmonic Au NPs may also exhibit characteristic short-time fluorescence, which depends on the surface roughness or the grain size effect [19]. In view of the above mentioned structural and optical features the Au NCs are potential candidates for being fluorescence markers, and their sensor applications are also in the focus of interest [4,20,21]. Protein-capped Au NCs have been successfully used for the detection of Hg^{2+} ions [22,23] where the LOD was assigned from the quantity of the fluorescence quenching. Several protein- or amino acid-capped Au NCs show high selectivity for Cu^{2+} ion,

too [24,25]. Besides copper, iron is also an essential trace element which has significant roles in oxygen transport or electron transfer. Therefore, the determination of the exact concentration of ferric ion is necessary. The iron content of drinking water must not exceed the maximal value of 200 μg dm^{-3} (*ca.* 3.58 μM) as established in the European Union regulation (Council Directive 98/83/EC of 3 November 1998 on the quality of water intended for human consumption). In previous publications copper NCs have been applied to detect ferric ions [26,27], so the utilization of Au NCs in the case of the development of selective anion and cation sensors is partially known [28–30]. The main goal of our work was to fabricate biocompatible AMP-stabilized Au NPs and Au NCs that have plasmonic or fluorescent features, respectively. Several excellent articles were published on protein- or peptide-stabilized NPs and NCs, but the application of nucleotides for the fabrication of gold colloids or nanosized clusters using simple biocompatible preparation route has been neglected. During the syntheses the AMP:$AuCl_4^-$ molar ratios of the formation of NPs and NCs were optimized. Moreover, the blue-emitting AMP-Au NCs have been utilized to develop a sensitive and selective sensor for Fe^{3+}. In the view of the K_{SV} and various thermodynamic parameters (ΔG, ΔH°, ΔS°) determined by the Stern-Volmer fitting of the fluorescence quenching, the mechanism of the quenching process was also supposed.

2. Experimental details

2.1. Materials

All chemicals were of analytical grade and were used without further purification. Adenosine 5'-monophosphate disodium salt ($C_{10}H_{12}N_5Na_2O_7P$, 99.0 %), gold(III) chloride acid trihydrate ($HAuCl_4\times3H_2O$, 99.9%), iron(III) chloride hexahydrate ($FeCl_3\times6H_2O$, 99.9%), manganese(II) chloride tetrahydrate ($MnCl_2\times4H_2O$, 98 %), cobalt(II) chloride hexahydrate ($CoCl_2\times6H_2O$, 98 %) nickel(II) chloride hexahydrate ($NiCl_2\times6H_2O$, 99 %), potassium chloride (KCl, >99%), copper chloride dihydrate ($CuCl_2\times2H_2O$, >98%) and sodium oxalate ($Na_2C_2O_4$, 99.5%) were purchased from Sigma-Aldrich. Citric acid monohydrate ($C_6H_8O_7\times H_2O$, 99.6 %), trisodium citrate dihydrate ($C_6H_5Na_3O_7\times2H_2O$, 99 %), zinc(II) chloride ($ZnCl_2$, 99.9 %), calcium chloride dihydrate ($CaCl_2\times2H_2O$, 97 %), magnesium chloride ($MgCl_2$, 98 %), sodium chloride (NaCl, 99 %), sodium bromide (NaBr, 99%), sodium hydrogencarbonate ($NaHCO_3$, 95%), sodium sulfate (Na_2SO_4, 95 %), sodium nitrate ($NaNO_3$, 99 %), sodium acetate (CH_3COONa, 99 %) and acetone (CH_3COCH_3, 99.9 %) were ordered from Molar. In all cases the stock solutions were freshly prepared using Milli-Q ultrapure water (18.2 MΩ·cm at 25 °C).

2.2. Preparation of AMP-Au NCs and AMP-Au NPs

1 mL of AMP aqueous solution (c = 10 mM) was mixed with 50 µL of $HAuCl_4$ aqueous solution (c = 10 mM) which corresponds to the AMP:$AuCl_4^-$ 20:1 molar ratio. The original intensive yellow color of the $AuCl_4^-$ was discolor on addition of AMP within a few minutes indicating the Au(III)/Au(I) reduction process. After 15 min of stirring 500 µL of citrate buffer solution (c = 0.5 M) was also added to this mixture to adjust the pH 6 and the final volume has been raised to 5 mL. The sample was thermostated for 24 h at 37 ºC. Finally, the synthesized AMP-Au NCs were purified by precipitation with acetone [31] and centrifugation (15000 rpm/30 min). After purification (removal of excess AMP), the Au NCs were redispersed in Milli-Q water. Similar preparation method was used for the fabrication of different AMP-Au NPs but the applied molar ratio of AMP:$AuCl_4^-$ was 1:1 in all dispersions and the concentrations of the precursor aurate were varied in the range of 0.5 – 5.0 mM. In the case of colloidal Au NPs the color of the samples was red wine at the end of the synthesis.

2.3. Characterization of the AMP-Au NCs and AMP-Au NPs

UV-Vis spectrophotometric studies have been performed by Shimadzu UV-1800 Spectrophotometer, using 1 cm quartz cuvette in the range of 190-800 nm, while the fluorescence spectra were recorded on Horiba, Jobin Yvon Fluoromax-4 instrument using 1 cm quartz cuvette at 335 nm excitation with 3 nm slit. The fluorescence lifetime and the quantum yields (QY %) of the AMP-Au NCs have been determined by using cresyl violet as reference by the Edinburgh Instruments FLSP920 time-resolved PL spectrometer using 378 nm excitation. The Fourier transform infrared (FT-IR) spectroscopic measurements in the middle range have been performed by using BIO-RAD Digilab Division FTS-65A/896 Fourier Transform infrared spectrometer with a Harrick's Meridian® SplitPea single-reflection diamond attenuated total reflectance (ATR) accessory. All IR spectra were measured at 4 cm^{-1} optical resolution, by averaging 256 interferrograms. The X-ray photoelectron spectroscopy (XPS) measurements were carried out by SPECS instrument equipped with a PHOIBOS 150 MCD 9 hemispherical analyzer. HRTEM images of the AMP-Au NPs were recorded on Tecnai G2 instrument at 200kV accelerating voltage and they were analyzed using ImageJ software. The DLS investigations have been performed with a Zetasizer Nano ZS ZEN 4003 apparatus (Malvern Inst., UK) equipped with a He-Ne laser (λ = 633 nm) at 25 ± 0.1 °C.

2.4. Fluorescence sensing of Fe^{3+} by using AMP-Au NCs

For sensing, 250-250 µL of purified AMP-Au NCs (c_{Au} = 0.1 mM) were added separately into 4.75 mL of aqueous solutions containing metal ions (K^+, Ca^{2+}, Mg^{2+}, Cu^{2+}, Zn^{2+}, Fe^{3+}, Mn^{2+}, Co^{2+}, Ni^{2+}) and anions (NO_3^-, HCO_3^-, SO_4^{2-}, Cl^-, Br^-, CH_2COO^-, $(COO)_2^{2-}$) where the concentration of the tested ions was constant (c_{ions} = 1.0 mM). The mixtures were incubated at room temperature for 1 min. The emission spectra of the blue-emitting Au NCs were recorded at room temperature both in the absence and in the presence of the added ions. For Fe^{3+} sensing, the quenching studies have been performed using several Fe^{3+} concentrations (from 100 nM to 1 mM) at four different temperatures (T = 298; 303; 313; 323 K) and the dynamic range was obtained. Based on temperature-dependent fluorescence studies the thermodynamic data (ΔG, ΔH°, ΔS°) of the quenching process have also been determined.

3. Results and discussion

3.1. The role of the AMP:$AuCl_4^-$ molar ratios in the structure and the optical features of the AMP-stabilized NPs and NCs

Depending on the molar ratios of the reactants (AMP/aurate ions) and on the applied Au concentrations AMP-Au NPs and AMP-Au NCs have been successfully fabricated. During our investigations we varied the AMP:$AuCl_4^-$ molar ratios as well as the gold concentrations in the range of 1:1 - 100:1 and 0.1-5.0 mM, respectively at 37 °C. Lopez and Liu had previously published that the spontaneous interactions of a simple adenine and its derivatives with aurate ions in aqueous solution result in the formation of fluorescent supramolecular Au(I)-complexes [32]. Furthermore, they also established that the application of citrate buffer plays a key role in the reduction process of aurate ions. Based on the previously published results in our work we have used citrate buffer to avoid the appearance of supramolecular complexes and to create a reductive medium. The synthesis was also carried out in the absence of citrate, but XPS results **(Fig. S1)** confirm that gold species containing Au(I) ($4f_{7/2}$ = 84.8 eV, $4f_{5/2}$ = 88.5 eV) and Au(III) ($4f_{7/2}$ = 86.7 eV, $4f_{5/2}$ = 90.5 eV) oxidation state are formed. In the course of the utilization of citrate buffer using AMP:$AuCl_4^-$ = 1:1 molar ratio AMP-stabilized colloidal Au dispersions were fabricated at 37 °C by using four different gold concentrations (c_{Au} = 0.5; 1.0; 2.0 and 5.0 mM, see **Fig. 1a**). Above 5.0 mM of Au concentration the appearance of aggregates was observed. The AMP-Au NPs have a

characteristic plasmon band at 525 nm [33] confirmed by UV-Vis spectroscopy (**Fig. 1a**). The prepared AMP-stabilized Au NPs showed good stability at room temperature even a few weeks later. The NPs have negative surface charge; the corresponding zeta potential is -23.2 ± 2.8 mV [34]. **Fig. 1b** presents a representative HRTEM image of the AMP-Au NPs using c_{Au} = 2.0 mM; we establish that the average size is 11.0 ± 1.8 nm. The parallel DLS measurements of this sample also support the formation of NPs with the average size of 11.1 ± 3.1 nm (polydispersity index (PDI) is 0.141). An increase in the gold concentration to 5.0 mM does not play a dominant role in the size of NPs; it was found that the average diameter randomly changed in the range of 9.6-11.7 nm. Contrary to the fabrication of NPs the syntheses of AMP-Au NCs were carried out by using a much lower gold concentration (c_{Au} = 0.1 mM) and several AMP:$AuCl_4^-$ ratios (from 1:1 to 1:100). It was established that the increase in the AMP excess results in the disappearance of the characteristic plasmon band at 525 nm as presented in **Fig. 2a** (blue line). The absorption maximum at 260 nm belongs to the purine ring of the AMP and the "shoulder" at 305 nm refers to the formation of the NCs [35]. In parallel with the disappearance of the plasmonic feature the samples show intensive fluorescence and it was also found that the PL intensity reaches the maximum at AMP:$AuCl_4^-$ = 20:1 ratio (**Fig. 2b**). Further increase in the AMP excess results in a decrease in the measured intensities. This characteristic PL belongs to ultra-small Au NCs stabilized by AMP. These AMP-Au NCs (prepared at 20:1 molar ratio) have characteristic fluorescence in the blue-range (at λ_{em} = 480 nm) using 335 nm excitation as presented in **Fig. 3a**. PL lifetime has been estimated and for two dominant species the values in the range of nanoseconds have been obtained (τ_1= 92 ns, α_1= 0.42; τ_2= 400 ns, α_2= 0.40). The polar environment for the fluorophore can increase the efficiency of the metal-ligand charge transfer between the NCs and the anchoring group of the surface ligand. Therefore, the longer lifetime component (τ_2) refers to the presence of this charge transfer. The average fluorescence lifetime is 200 ns and the QY (%) is 0.9 %. The PL decay profile of the AMP-Au NCs with the corresponding residuals is presented in **Fig. 3b**. Both the location of the emission maximum (in the blue range) and the PL lifetime and QY(%) data strongly indicate the formation of subnanometer-sized luminescent Au NCs [14].

3.2. Structural characterization and stability investigations of the AMP-Au NCs

The registered infrared and the XPS spectra are presented in **Fig. 4**. The middle range (1800-1000 cm^{-1}) of IR spectrum (**Fig. 4a**) contains several information on the primary coordination of metal [36]. It was observed that the -NH_2 bending vibration of adenine is shifted to the

lower wavenumber in the NCs (**1**: from 1583 cm^{-1} to 1563 cm^{-1}). Additionally, the stretching vibration of N3-C2, N1-C2 and N7-C5 bindings (**2**) in the purine ring measurably shifted to the higher wavenumber (from 1329 cm^{-1} to 1375 cm^{-1}). The shifts of these bonds refer to the Au coordination to the purine ring (**Fig. S2**). The -NH_2 group of the purine ring (N7 position in AMP) has high-affinity to bind the metal ions [37]. The bending vibration of N9-H and C8-H bonds (**3**: from 1068 cm^{-1} to 1078 cm^{-1}) and the stretching vibration of C5'-O (**4**: from 1034 cm^{-1} to 1060 cm^{-1}) are also drifted which indicate the conformational change of the AMP molecules. The XPS measurement (see **Fig. 4b**) strongly denotes the formation of subnanometer sized Au NCs due to the binding energies detected at Au $4f_{7/2}$ = 84.6 eV and $4f_{5/2}$ = 88.3 eV. In the case of bulk gold the peak maximum of Au^0 $4f_{7/2}$ is located at around ~ 84 eV [38] and the spectrum shows well-defined sharp peaks. In contrast, for nanosized particles the above mentioned peak maximum (Au $4f_{7/2}$) locates between 84.2 and 84.8 eV depending on the size and structure of the clusters. Furthermore, the broadening of the XPS peak is also observable parallel with the decrease of the cluster size. Besides the structural characterization the pH-stability of the AMP-Au NCs has also been investigated in a wide pH range (pH 1-12). As it can be seen in **Fig. S3a**, below pH 6.0 and above pH 9.0 the fluorescence intensity of the AMP-Au NCs continually decreases. This observation is in good agreement with the change of the size and the Zeta-potential values of the nanoclusters determined by DLS. The hydrodynamic diameter of the AMP-Au NCs is 0.71 ± 0.1 nm (PDI = 0.181) at pH 6.0. Fig. S3b clearly represents that in the pH range of 6.0-9.0 the size does not change measurable and the Zeta potential values are in the range of -35 – (-25) mV indicating the presence of stabile system. Below pH 6 the size of these clusters starts to increase and the absolute value of Zeta-potentials also decreases to 5-10 mV which confirm the formation of aggregated particles at acidic conditions. At strong acidic media (pH 1-2) fast aggregation was also observed, which is followed by DLS studies. The measured hydrodynamic diameter gradually increases in time (**Fig. S4**). In conclusion we established that synthesized blue-emitting AMP-Au NCs show high kinetic stability in the pH range of 6.0-9.0, where the PL intensity, the size and the Zeta-potential values are nearly constant. In addition, the change of the temperature (samples stored at 4 °C or at 37°C) or the addition of sodium chloride to the NCs-containing aqueous dispersion has no dominant influence on the measured fluorescence intensity.

3.3. Fluorescent sensing of Fe^{3+}

Numerous metal ions (K^+, Ca^{2+}, Mg^{2+}, Cu^{2+}, Zn^{2+}, Fe^{3+}, Mn^{2+}, Co^{2+}, Ni^{2+}) and anions (NO_3^-, HCO_3^-, SO_4^{2-}, Cl^-, Br^-, CH_3COO^-, $(COO)_2^{2-}$) were tested as fluorescence quencher, but the disappearance of the emission band of the AMP-Au NCs is observed only for the addition of Fe^{3+} ion (**Fig. 5** and **Fig. S5**). Contrary to the studied cations and anions a significant decrease ($I_0/I > 2$) in the fluorescence intensity of the emission peak at λ_{em} = 480 nm was detected for Fe^{3+} ion, where the $I_0/I > 30$ is established (**Fig. 5a** and **b**). The LOD was 2 µM (the signal/noise (S/N) ratio is greater than 3). This LOD value is slightly lower than the permissible value of the iron in tap water so our developed Au NCs-based sensor are able to detect immediately the Fe^{3+} content in drinking water if the concentration approaches the limit value of *ca*. 3.5 µM. PL quenching of AMP-Au NCs was also observed in the presence of I^- but the detection limit was measurable higher than in the case of Fe^{3+}. It was also found that there is a linear relationship between fluorescence quenching and the concentration of Fe^{3+} within a range from 10 µM to 100 µM **(Fig. 6a** and **b)**. Based on the Stern-Volmer fitting [39] of the fluorescence data the quenching constant (K_{SV}) can be determined according to the **Eq. 1**, where $\boldsymbol{I_0}$ and $\boldsymbol{I}$ is the maximum of the fluorescence intensity before and after the addition of Fe^{3+} and [Q] is the equilibrium concentration of Fe^{3+}.*

$$I_0/I = 1 + K_{SV}[Q] \quad (1)$$

If we plotted the I_0/I as a function of c_{Fe3+} **(Fig. 6b)** the slope of the curve gives the corresponding K_{SV}. Using the modified Stern-Volmer equation (**Eq. 2**) [40] the K_a binding constants were also calculated ($I_0/(I_0-I)$ vs. $[Q]^{-1}$) and the values were summarized in **Table 1**.

$$I_0/\Delta I = 1/f_a + 1/f_a K_a [Q]^{-1} \quad (2)$$

where the $\boldsymbol{\Delta I = I_0 - I}$, $\boldsymbol{f_a}$ is the mole fraction of solvent accessible AMP-Au NCs, $\boldsymbol{K_a}$ is analogous to the associative binding constant. In view of the K_a the Gibbs free energy change (ΔG) can be determined on the basis of the well-known $\Delta G = -RT\ln K_a$ correlation, where $\boldsymbol{R}$ is the gas constant, $\boldsymbol{T}$ is the absolute temperature. If the measurements were carried out at different temperatures based on the integrated form of the van't Hoff equation (**Eq. 3**) certain thermodynamic parameters such as enthalpy change ($\Delta H°$), entropy change ($\Delta S°$) and the heat capacity change (ΔC_p) will also be given [41].

* If the value of K_{SV} is large enough and the Stern-Vollmer plot is linear instead of the equilibrium concentration of the quencher the analytical concentration is also useable.

$$lnK_a = -{}^{\Delta H^0(T^0)}/_{RT} + {}^{\Delta S^0(T^0)}/_{R} + {}^{\Delta C_p}/_{R}\left[\left(T - {}^{T^0}/_{T}\right) - ln\,{}^{T}/_{T^0}\right] \quad (3)$$

In this work the quenching studies were carried out at 298 (**Fig. 6a and b**), 303 (**Fig. S6**), 310 (**Fig.S7**) and 323 (**Fig. S8**) K as well and the calculated lnK_a values as a function of reciprocal temperature are presented in **Fig. 7a**. The determined thermodynamic data are summarized in **Table 1** based on the integrated van't Hoff analysis (**Eq. 3**). **Fig.7a**. shows that linear (grey dashed line) and nonlinear (black dashed line) regression methods were also used to fit the experimental data [41]. It was found that instead of the widely applied linear regression, in our case the nonlinear regression method provides the best correlation of the experimental data. Namely, in the case of the linear regression the calculated coefficient is 0.9022 while for nonlinear regression the coefficient is 0.9823. The negative values of ΔG (*ca*. -29 kJ mol^{-1} depending on the temperature) indicate that the reactions between the AMP-Au NCs and Fe^{3+} ions are thermodynamically favorable. The negative ΔH° (-84.57±8.46 kJ mol^{-1}) suggests the fact that the binding reaction is exothermic. Since, it was established that the ΔH° < 0 and ΔS° < 0 and also the |ΔH°| > |TΔS°| most probably the reaction is spontaneous and is enthalpy-driven [35]. The detemined ΔC_p is -4.86±1.17 kJ $mol^{-1}K^{-1}$. As **Fig. 7b** shows that neither the citrate nor the pure AMP form a colored complex with Fe^{3+}; an absorption band at 480 nm (where the cluster has a characteristic emission band) is not detected in the UV-Vis spectra indicating that the self-absorption has not occurred. Several articles have been published on the metal binding capability of nucleotides [42,43] and based on these articles the quenching most probably derives from the interaction between the AMP molecules (e.g. purine ring) located on the cluster surface and the Fe^{3+} ions. The Zeta-potential values of the clusters before (ca. -35 mV) and after (ca. + 30 mV) addition of Fe^{3+} ions also confirm the strong binding of metal ions onto the cluster surface (Fig. 5.a). Based on the defined parameters it can be seen that the K_{SV} has decreased with an increase in the temperature, which refers to static quenching. In the case of static quenching non-fluorescent (dark) complexes are formed between the fluorophore on ground state and the quencher, and the number of fluorescent molecules is decreased in the excited state [44].

4. Conclusions

In summary, we have first demonstrated the AMP-directed synthesis of both colloidal Au NPs and fluorescent Au NCs using a simple fabrication route. The dominant role of the molar ratios of the reactants has been proved in relation to the size as well as to the unique optical

features of the prepared gold nanosized products. The relatively monodispersed AMP-Au NPs (d ~ 11 nm) fabricated at 37°C via biocompatible preparation route showed high stability at room temperature even a few weeks later. The ultra-small blue-emitting AMP-Au NCs also possess high stability in aqueous medium between pH 6.0-9.0 regardless of the temperature and the physiological salt concentration. These AMP-Au NCs have been used to develop a rapid, selective and sensitive sensor for the detection of Fe^{3+} ions. The dynamic range (10-100 µM) and the LOD (2.0 µM) have been obtained and some important physico-chemical quantities of the interaction can also be provided. These water-soluble, stabile, blue-emitting AMP-Au NCs synthesized via reproducible preparation approach are suitable for the fabrication of iron selective, "turn off" chemosensors.

Acknowledgement

The research was supported by the National Research, Development and Innovation Office-NKFIH through the project "Synthesis, structural and thermodynamic characterization of nanohybrid systems at solid-liquid interfaces" K116323 and GINOP-2.3.2-15-2016-00038 and GINOP-2.3.2-15-2016-00013. The authors thank Péter Baranyai (MTA TTK, Budapest, Hungary) for the PL lifetime and QY(%) measurement and Erika Varga (University of Szeged, Department of Physical Chemistry and Materials Sciences) for the XPS studies.

References

[1] X. Huang, M.A. El-Sayed, Gold nanoparticles: Optical properties and implementations in cancer diagnosis and photothermal therapy, J. Adv. Res. 1 (2010) 13–28.

[2] Y. Li, H.J. Schluesener, S. Xu, Gold nanoparticle-based biosensors, Gold Bull. 43 (2010) 29–41.

[3] L. Dykman, N. Khlebtsov, Gold nanoparticles in biomedical applications: recent advances and perspectives., Chem. Soc. Rev. 41 (2012) 2256–2282.

[4] L. Shang, G.U. Nienhaus, Gold nanoclusters as novel optical probes for in vitro and in vivo fluorescence imaging, Biophys. Rev. 4 (2012) 313–322.

[5] S. Liu, F. Lu, J.-J. Zhu, Highly fluorescent Ag nanoclusters: microwave-assisted green synthesis and Cr3+ sensing, Chem. Commun. 47 (2011) 2661.

[6] L. Polavarapu, M. Manna, Q.-H. Xu, Biocompatible glutathione capped gold clusters as one- and two-photon excitation fluorescence contrast agents for live cells imaging., Nanoscale. 3 (2011) 429–434.

[7] L. Shang, F. Stockmar, N. Azadfar, G.U. Nienhaus, Intracellular thermometry by using fluorescent gold nanoclusters, Angew. Chemie - Int. Ed. 52 (2013) 11154–11157.

[8] L. Polavarapu, Q.-H. Xu, A single-step synthesis of gold nanochains using an amino acid as a capping agent and characterization of their optical properties., Nanotechnology. 19 (2008) 75601.

[9] E. Csapó, D. Ungor, Á. Juhász, G.K. Tóth, I. Dékány, Gold nanohybrid systems with tunable fluorescent feature: Interaction of cysteine and cysteine-containing peptides with gold in two- and three-dimensional systems, Colloids Surfaces A Physicochem. Eng. Asp. 511 (2016) 264–271.

[10] J. Xie, Y. Zheng, J.Y. Ying, Protein-directed synthesis of highly fluorescent gold nanoclusters., J. Am. Chem. Soc. 131 (2009) 888–9.

[11] V. Hornok, E. Csapó, N. Varga, D. Ungor, D. Sebők, L. Janovák, G. Laczkó, I. Dékány, Controlled syntheses and structural characterization of plasmonic and red-emitting gold/lysozyme nanohybrid dispersions, Colloid Polym. Sci. 294 (2016) 49–58.

[12] F. Kretschmer, U. Mansfeld, S. Hoeppener, M.D. Hager, U.S. Schubert, Tunable synthesis of poly(ethylene imine)–gold nanoparticle clusters, Chem. Commun. 50 (2014) 88–90.

[13] H. Kawasaki, K. Hamaguchi, I. Osaka, R. Arakawa, pH-dependent synthesis of pepsin-mediated gold nanoclusters with blue green and red fluorescent emission, Adv. Funct. Mater. 21 (2011) 3508–3515.

[14] J. Zheng, C. Zhou, M. Yu, J. Liu, Different sized luminescent gold nanoparticles, Nanoscale. 4 (2012) 4073.

[15] S. Fedrigo, W. Harbich, J. Buttet, Optical response of Ag2, Ag3, Au2, and Au3 in argon matrices, J. Chem. Phys. 99 (1993) 5712–5717.

[16] J. Zheng, P.R. Nicovich, R.M. Dickson, Highly fluorescent noble-metal quantum dots., Annu. Rev. Phys. Chem. 58 (2007) 409–431.

[17] Y. Negishi, K. Nobusada, T. Tsukuda, Glutathione-Protected Gold Clusters Revisited: Bridging the Gap between Gold(I)−Thiolate Complexes and Thiolate-Protected Gold Nanocrystals, J. Am. Chem. Soc. 127 (2005) 5261–5270.

[18] Z. Tang, D.A. Robinson, N. Bokossa, B. Xu, S. Wang, G. Wang, Mixed dithiolate Durene-DT and monothiolate phenylethanethiolate protected Au130 nanoparticles with discrete core and core-ligand energy states, J. Am. Chem. Soc. 133 (2011) 16037–16044.

[19] C. Zhou, J. Yu, Y. Qin, J. Zheng, Grain size effects in polycrystalline gold nanoparticles, Nanoscale. 4 (2012) 4228.

[20] P. Bian, J. Zhou, Y. Liu, Z. Ma, One-step fabrication of intense red fluorescent gold nanoclusters and their application in cancer cell imaging, Nanoscale. 5 (2013) 6161–6166.

[21] X. Guo, F. Wu, Y. Ni, S. Kokot, Synthesizing a nano-composite of BSA-capped Au nanoclusters/graphitic carbon nitride nanosheets as a new fluorescent probe for dopamine detection, Anal. Chim. Acta. 942 (2016) 112–120.

[22] H. Wei, Z. Wang, L. Yang, S. Tian, C. Hou, Y. Lu, Lysozyme-stabilized gold fluorescent cluster: Synthesis and application as Hg(2+) sensor., Analyst. 135 (2010) 1406–1410.

[23] D. Lu, C. Zhang, L. Fan, H. Wu, S. Shuang, C. Dong, A novel ratiometric fluorescence probe based on BSA assembled silver nanoclusters for mercuric ion selective sensing, Anal. Methods. 5 (2013) 5522.

[24] Y. Xu, X. Yang, S. Zhu, Y. Dou., Selectively fluorescent sensing of Cu2+ based on lysine-functionalized gold nanoclusters, Colloids Surfaces A Physicochem. Eng. Asp. 450 (2014) 115–120.

[25] Z. Lin, F. Luo, T. Dong, L. Zheng, Y. Wang, Y. Chi, G. Chen, Recyclable fluorescent gold nanocluster membrane for visual sensing of copper(II) ion in aqueous solution., Analyst. 137 (2012) 2394–9.

[26] J. Feng, Y. Ju, J. Liu, H. Zhang, X. Chen, Polyethyleneimine-templated copper

nanoclusters via ascorbic acid reduction approach as ferric ion sensor, Anal. Chim. Acta. 854 (2015) 153–160.

[27] H. Huang, H. Li, J.-J. Feng, H. Feng, A.-J. Wang, Z. Qian, One-pot green synthesis of highly fluorescent glutathione-stabilized copper nanoclusters for Fe3+ sensing, Sensors Actuators B Chem. 241 (2017) 292–297.

[28] J.A. Annie Ho, H.C. Chang, W.T. Su, DOPA-mediated reduction allows the facile synthesis of fluorescent gold nanoclusters for use as sensing probes for ferric ions, Anal. Chem. 84 (2012) 3246–3253.

[29] X. Mu, L. Qi, P. Dong, J. Qiao, J. Hou, Z. Nie, H. Ma, Facile one-pot synthesis of l-proline-stabilized fluorescent gold nanoclusters and its application as sensing probes for serum iron, Biosens. Bioelectron. 49 (2013) 249–255.

[30] Q. Zhao, H. Yan, P. Liu, Y. Yao, Y. Wu, J. Zhang, H. Li, X. Gong, J. Chang, An ultra-sensitive and colorimetric sensor for copper and iron based on glutathione-functionalized gold nanoclusters, Anal. Chim. Acta. 948 (2016) 73–79.

[31] J.P. Vanegas, E. Zaballos-García, M. González-Béjar, P. Londoño-Larrea, J. Pérez-Prieto, Adenosine monophosphate-capped gold(<scp>i</scp>) nanoclusters: synthesis and lanthanide ion-induced enhancement of their luminescence, RSC Adv. 6 (2016) 17678–17682.

[32] A. Lopez, J. Liu, Light-activated metal-coordinated supramolecular complexes with charge-directed self-assembly, J. Phys. Chem. C. 117 (2013) 3653–3661.

[33] A. Majzik, L. Fülöp, E. Csapó, F. Bogár, T. Martinek, B. Penke, G. Bíró, I. Dékány, Functionalization of gold nanoparticles with amino acid, β-amyloid peptides and fragment, Colloids Surfaces B Biointerfaces. 81 (2010) 235–241.

[34] E. Csapó, D. Sebők, J. Makrai Babić, F. Šupljika, G. Bohus, I. Dékány, N. Kallay, T. Preočanin, Surface and Structural Properties of Gold Nanoparticles and Their Biofunctionalized Derivatives in Aqueous Electrolytes Solution, J. Dispers. Sci. Technol. 35 (2014) 815–825.

[35] H.H. Deng, F.F. Wang, X.Q. Shi, H.P. Peng, A.L. Liu, X.H. Xia, W. Chen, Water-soluble gold nanoclusters prepared by protein-ligand interaction as fluorescent probe for real-time assay of pyrophosphatase activity, Biosens. Bioelectron. 83 (2016) 1–8.

[36] J. Kundu, O. Neumann, B.. Janesko, D. Zhang, S. Lal, a Barhoumi, G.E. Scuseria, N.J. Halas, Adenine− and Adenosine Monophosphate (AMP)− Gold Binding Interactions Studied by Surface-Enhanced Raman and Infrared Spectroscopies, J. Phys. Chem. C. 113 (2009) 14390–14397.

[37] J. Liu, DNA-stabilized, fluorescent, metal nanoclusters for biosensor development, TrAC Trends Anal. Chem. 58 (2014) 99–111. doi:10.1016/j.trac.2013.12.014.

[38] S. Peters, S. Peredkov, M. Neeb, W. Eberhardt, M. Al-Hada, Size-dependent XPS spectra of small supported Au-clusters, Surf. Sci. 608 (2013) 129–134.

[39] G. Zhang, Q. Que, J. Pan, J. Guo, Study of the interaction between icariin and human serum albumin by fluorescence spectroscopy, J. Mol. Struct. 881 (2008) 132–138.

[40] S. Huang, H. Qiu, Y. Liu, C. Huang, J. Sheng, W. Su, Q. Xiao, Molecular interaction investigation between three CdTe:Zn(2+) quantum dots and human serum albumin: A comparative study., Colloids Surf. B. Biointerfaces. 136 (2015) 955–62.

[41] Á. Juhász, E. Csapó, D. Ungor, G.K. Tóth, L. Vécsei, I. Dékány, Kinetic and Thermodynamic Evaluation of Kynurenic Acid Binding to GluR1 270–300 Polypeptide by Surface Plasmon Resonance Experiments, J. Phys. Chem. B. 120 (2016) 7844–7850.

[42] C.M. Mikulski, S. Cocco, N. De Franco, T. Moore, N.M. Karayannis, Adenine complexes with divalent 3d metal chlorides, Inorganica Chim. Acta. 106 (1985) 89–95.

[43] R. Ghose, Metal Complexation with Adenine and Thymine, Synth. React. Inorg. Met. Chem. 22 (1992) 379–392.

[44] E.M. Talavera, B. Quintero, J.M. Alvarez, Static and dynamic fluorescence quenching of carbazole by tropanic alkaloids, J. Photochem. Photobiol. A Chem. 66 (1992) 171–184.

Figure and Table Captions

Fig. 1 (a) Representative plasmon band of AMP-Au NPs using c_{Au} = 2 mM with the photos of the Au colloidal dispersions prepared at four different Au concentrations. (b) HRTEM image of AMP-Au NPs at c_{Au} = 2 mM.

Fig. 2 (a) The UV-Vis spectra of gold(III) chloride (dashed grey line), AMP (dashed black line) and AMP-Au NCs (blue line) using 20:1 molar ratio (c_{Au} = 0.1 mM). (b) Fluorescence intensities of the emission bands (λ_{em} = 480 nm, λ_{ex} = 335 nm) of different AMP:$AuCl_4^-$ systems as a function of AMP concentration with a photo of the aqueous sample at AMP:$AuCl_4^-$ = 20:1 ratio (c_{Au} = 0.1 mM).

Fig. 3 (a) The excitation (grey line) and the emission (black line) bands of AMP-Au NCs. (b) The photoluminescence decay profile of the AMP-Au NCs. (c_{Au} = 0.1 mM, AMP:$AuCl_4^-$ = 20:1)

Fig. 4 (a) FT-IR spectra of the pure AMP (black) and the lyophilized powder of AMP-Au NCs 20:1 (grey). (b) XPS spectrum of the AMP-Au NCs 20:1.

Fig. 5 (a) Zeta-potential values of the AMP-Au NCs before and after addition of the investigated cations (c_{ions} = 1.0 mM), relative emission intensity (I_0/I) of the AMP-Au NCs after the addition of 1 mM concentrations of different (b) metal ions and (c) anions. Photographs of AMP-Au NCs under UV-lamp before and after the addition of 1 mM of Fe^{3+} ions.

Fig. 6 (a) Emission spectra of the AMP-Au NCs with increasing concentrations of Fe^{3+} ions in the dynamic range (from 10 µM to 100 µM) at 25 ºC. (b) The Stern-Volmer-fitting of the fluorescence quenching data according to Eq. 1. The standard deviation is ± 5 %.

Fig. 7 (a) The van't Hoff plot (linear fitting: grey line, non-linear fitting: black line) for the interaction between AMP-Au NCs and Fe^{3+} ions. (b) UV-Vis spectra of the (1) AMP/Fe^{3+}, (2) citrate/Fe^{3+}, (3) pure Fe^{3+}, (4) pure AMP and (5) pure citrate systems under the same concentrations as used for sensor measurements. The (6) represents the PL spectrum of AMP-Au NCs 20:1.

Table 1. The Stern-Volmer constant, the binding constants and the relative thermodynamic parameters of the Fe^{3+}-induced quenching of the AMP-Au NCs at different temperatures.

Figures

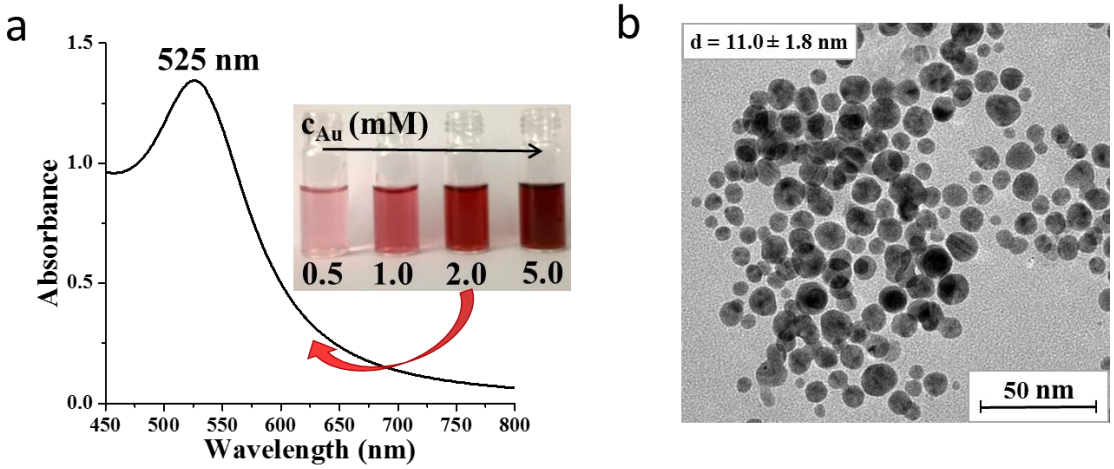

Figure 1.

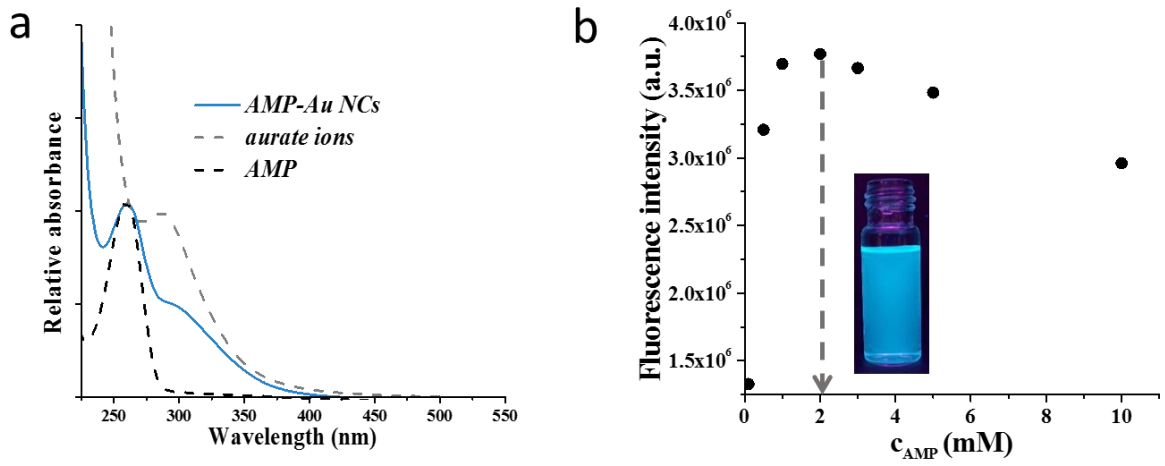
a
Relative absorbance
AMP-Au NCs
aurate ions
AMP
250
300
350
400
450
500
550
Wavelength (nm)
b
Fluorescence intensity (a.u.)
4.0x10^6
3.5x10^6
3.0x10^6
2.5x10^6
2.0x10^6
1.5x10^6
0
2
4
6
8
10
c_AMP (mM)

Figure 2.

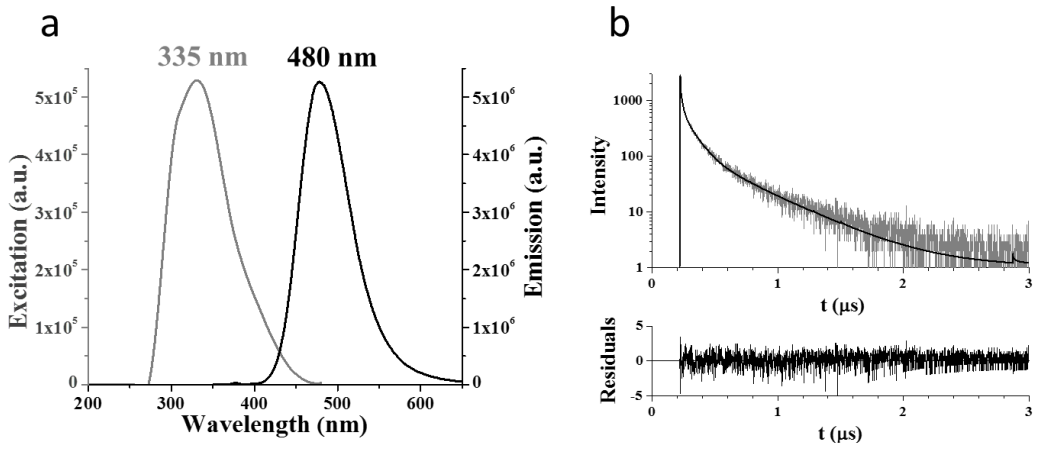
a
335 nm
480 nm
Excitation (a.u.)
Emission (a.u.)
Wavelength (nm)
b
Intensity
t (μs)
Residuals
t (μs)

Figure 3.

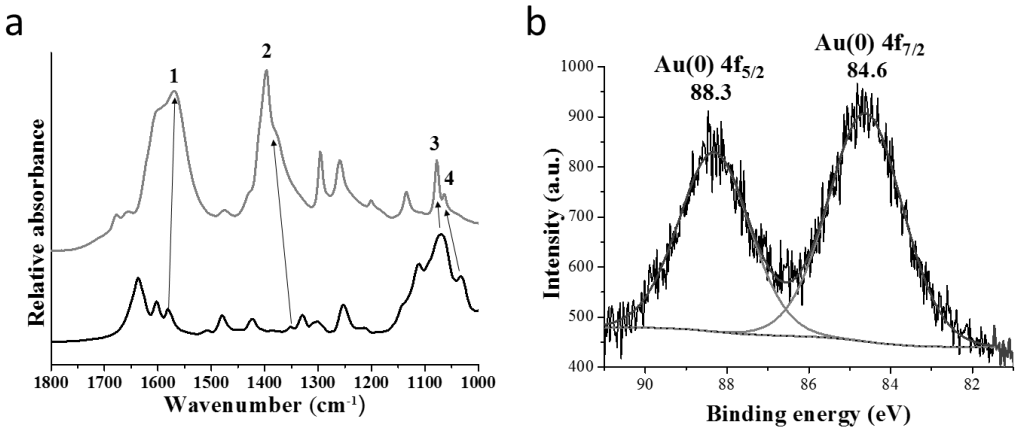
a
1
2
3
4
Relative absorbance
1800 1700 1600 1500 1400 1300 1200 1100 1000
Wavenumber (cm-1)
b
Au(0) 4f5/2
88.3
Au(0) 4f7/2
84.6
Intensity (a.u.)
1000 900 800 700 600 500 400
90 88 86 84 82
Binding energy (eV)

Figure 4.

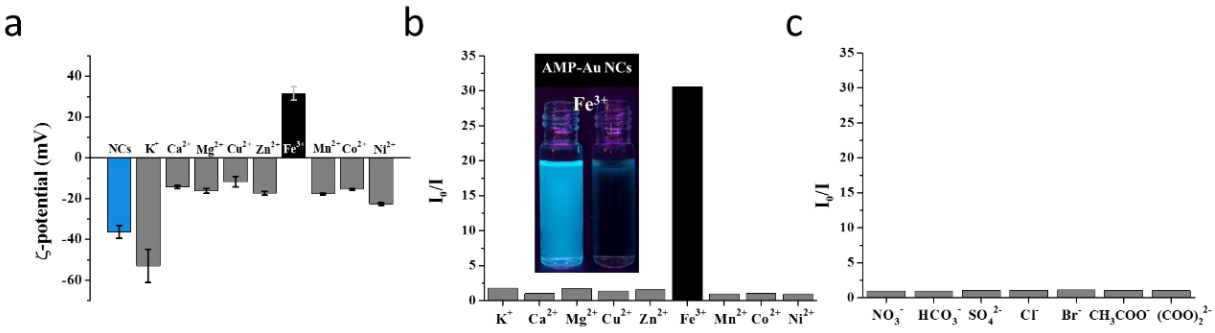
a
b
c
ζ-potential (mV)
NCs
K+
Ca2+
Mg2+
Cu2+
Zn2+
Fe3+
Mn2+
Co2+
Ni2+
I0/I
AMP-Au NCs
Fe3+
NO3-
HCO3-
SO4 2-
Cl-
Br-
CH3COO-
(COO)2 2-

Figure 5.

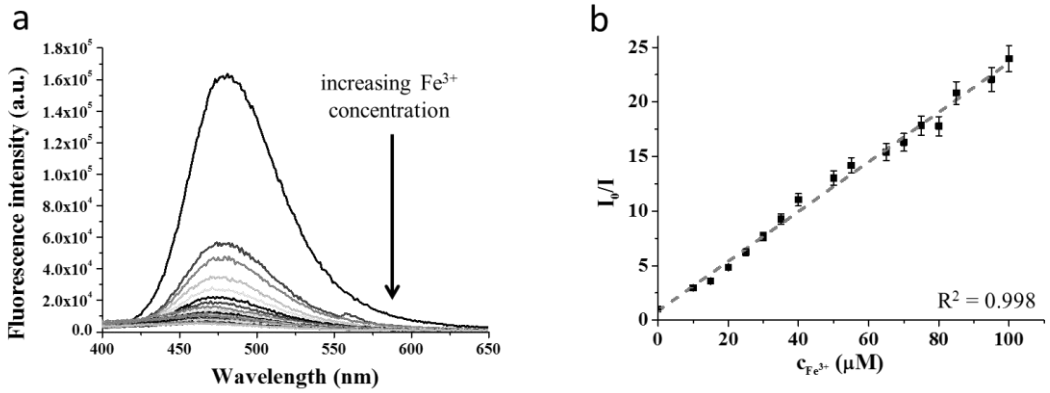
a
Fluorescence intensity (a.u.)
1.8x10^5
1.6x10^5
1.4x10^5
1.2x10^5
1.0x10^5
8.0x10^4
6.0x10^4
4.0x10^4
2.0x10^4
0.0
400
450
500
550
600
650
Wavelength (nm)
increasing Fe3+
concentration
b
I0/I
25
20
15
10
5
0
0
20
40
60
80
100
cFe3+ (μM)
R2 = 0.998

Figure 6.

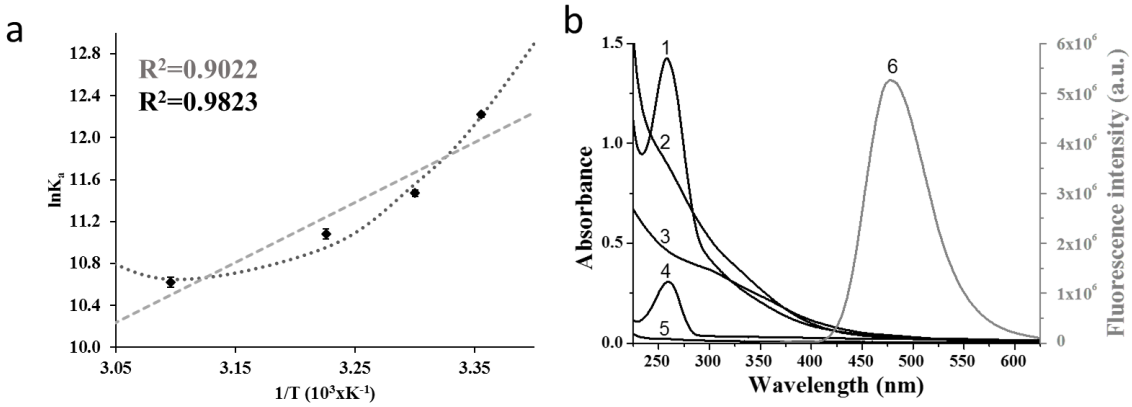
a
R²=0.9022
R²=0.9823
lnK_a
1/T (10³xK⁻¹)
b
Absorbance
Fluorescence intensity (a.u.)
Wavelength (nm)
1
2
3
4
5
6

Figure 7.

Table 1

T (K)	K_{SV} ($dm^3\ mol^{-1}$)	K_a ($dm^3\ mol^{-1}$)	SD[a]	R[b]	ΔG (kJ mol^{-1})	ΔH° (kJ mol^{-1})	ΔS° (kJ $mol^{-1}\ K^{-1}$)
298	237000	203000	5000	0.998	-30.28±0.81	-84.57±8.46	-0.183±0.03
303	112000	96000	3000	0.981	-28.90±0.83		
310	73000	65000	3000	0.949	-28.56±0.87		
323	49000	41000	2000	0.929	-28.52±0.93		

[a] standard deviations of the K_{SV}

[b] correlation coefficients for K_{SV}

Nucleotide-directed syntheses of gold nanohybrid systems with structure-dependent optical features: Selective fluorescence sensing of Fe^{3+} ions

Ditta Ungor[a], Edit Csapó[a,b,*], Barbara Kismárton[a], Ádám Juhász[a,b], Imre Dékány[a,*]

[a] MTA-SZTE Supramolecular and Nanostructured Materials Research Group, Department of Medical Chemistry, Faculty of Medicine, University of Szeged, H-6720 Dóm square 8, Szeged, Hungary

[b] Department of Physical Chemistry and Materials Sciences, University of Szeged, H-6720, Aradi v.t.1, Szeged, Hungary

Graphical abstract

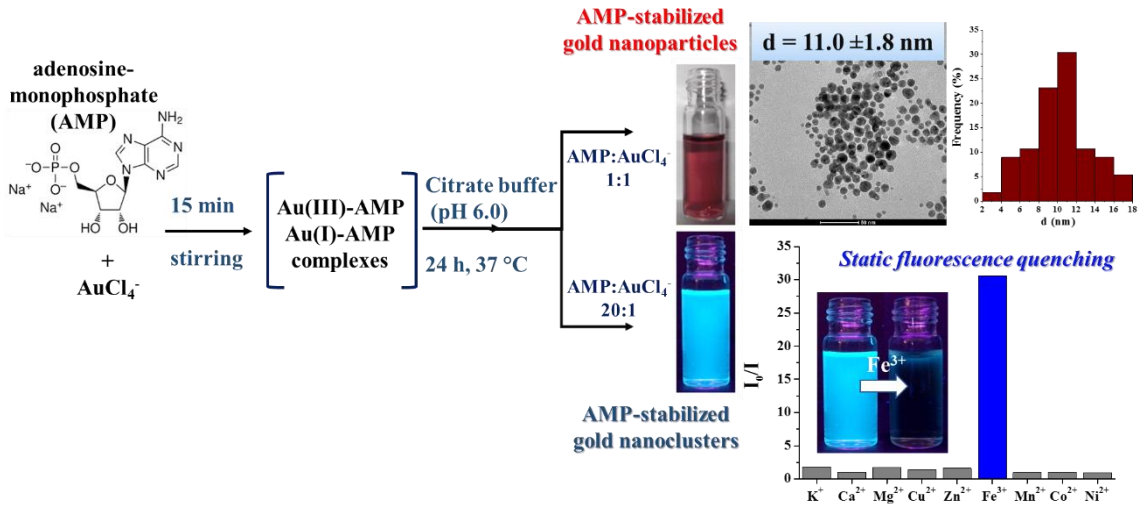

Preparation routes of AMP-stabilized gold nanoparticles and nanoclusters

Supplementary Material

Click here to download Supplementary Material: Revised Supplementary marc18.docx